Elastic, inelastic, and 1-nucleon transfer channels in the ^{7}Li + ^{120}Sn system

A. Kundu,[1,2,*] S. Santra,[1,2] A. Pal,[1,2] D. Chattopadhyay,[1,2] R. Tripathi,[2,3] B. J. Roy,[1,2] T. N. Nag,[3] B. K. Nayak,[1,2] A. Saxena,[1,2] and S. Kailas[1,2]

[1]*Nuclear Physics Division, Bhabha Atomic Research Centre, Mumbai 400085, India*

[2]*Homi Bhabha National Institute, Anushakti Nagar, Mumbai 400094, India*

[3]*Radiochemistry Division, Bhabha Atomic Research Centre, Mumbai 400085, India*

(Received 26 December 2016; revised manuscript received 24 February 2017; published 30 March 2017)

Background: Simultaneous description of major outgoing channels for a nuclear reaction by coupled-channels calculations using the same set of potential and coupling parameters is one of the difficult tasks to accomplish in nuclear reaction studies.

Purpose: To measure the elastic, inelastic, and transfer cross sections for as many channels as possible in ^{7}Li + ^{120}Sn system at different beam energies and simultaneously describe them by a single set of model calculations using FRESCO.

Methods: Projectile-like fragments were detected using six sets of Si-detector telescopes to measure the cross sections for elastic, inelastic, and 1-nucleon transfer channels at two beam energies of 28 and 30 MeV. Optical model analysis of elastic data and coupled-reaction-channels (CRC) calculations that include around 30 reaction channels coupled directly to the entrance channel, with respective structural parameters, were performed to understand the measured cross sections.

Results: Structure information available in the literature for some of the identified states did not reproduce the present data. Cross sections obtained from CRC calculations using a modified but single set of potential and coupling parameters were able to describe simultaneously the measured data for all the channels at both the measured energies as well as the existing data for elastic and inelastic cross sections at 44 MeV.

Conclusions: Non-reproduction of some of the cross sections using the structure information available in the literature which are extracted from reactions involving different projectiles indicates that such measurements are probe dependent. New structural parameters were assigned for such states as well as for several new transfer states whose spectroscopic factors were not known.

DOI: 10.1103/PhysRevC.95.034615

I. INTRODUCTION

Heavy-ion peripheral reactions, like inelastic excitations and transfer processes, offer a spectroscopic tool for the excitation of high-spin states of stable as well as unstable nuclei and complex nuclear configurations such as single-particle states coupled to core vibrational states [1]. For such direct reactions, the dynamics of the interactions are often governed by structural parameters of the participating nuclei, which determine the coupling to the entrance channel and influence the resulting cross sections of all open channels. Simultaneous description of such dominant outgoing channels by the same coupled channels calculations using same set of potential and coupling parameters is one of the difficult tasks in nuclear reaction studies, and is an important tool that reveals realistic structural parameters for that projectile-target system. In the present study, differential cross sections for elastic and inelastic scattering and one-nucleon transfer reactions have been measured for ^{7}Li + ^{120}Sn at 28- and 30-MeV beam energies, and a simultaneous description of these channels has been attempted by means of explicit coupled-reaction-channels (CRC) calculations in the distorted-wave Born approximation (DWBA) limit, with a consistent set of potential parameters as well as coupling parameters. The motivation is to extract realistic energy-independent structural information for the dominant nonelastic channels with the same set of model calculations that are important for characterizing also the other reaction channels of a system, for instance, fusion. Studies with similar reactions with weakly bound unstable nuclei, e.g., ^{11}Be or ^{11}Li [2–6], where coupled-channels effects are an issue, are of tremendous interest. Measurements with weakly bound stable nuclei, with better understood structures, are relatively easier, due to the higher beam intensities. The understanding of the reaction mechanisms for these projectiles acts as a reference for studies with unstable projectiles that are expected to be of similar complexity.

Inelastic transitions in a nucleus are caused by electromagnetic and/or nuclear interactions with another nucleus. As shown in Ref. [7], the transition amplitude for nuclear inelastic scattering is closely analogous to the electric multipole operator, $E\lambda$, where λ is the multipolarity of the excitation, except that the former involves the matter density while the latter is sensitive only to the charge density of the nucleus [8,9]. The quantity

$$B(E\lambda, J_i \rightarrow J_f) = \frac{1}{2J_i + 1} |\langle J_f || E\lambda || J_i \rangle| \quad (1)$$

is the reduced electromagnetic transition probability related to Coulomb deformation of the nucleus, commonly measured via γ-ray transitions from nuclear excited states, and the rate of very forward-angle (or low-energy) Coulomb excitation

*ananyak.delhi@gmail.com

reactions depends only on this structural property [10]. Here, J_f and J_i are the total spins of the final and initial states, respectively, which define the transition matrix element for the $E\lambda$ operator. In Coulomb-dominated heavy-ion scattering processes, $B(E\lambda)$ acts as a reliable structural information that connects theory and experiment. As smaller distances are approached (larger scattering angles), the nuclear force comes into the picture. Consequently, the nuclear amplitude changes faster than the Coulomb amplitude. Therefore, it is possible to determine Coulomb and nuclear deformations separately by measuring the angular distribution at both forward and backward angles [11]. The characteristics of the dominant multipole transitions (mainly quadrupole and octupole) between the low-lying first excited states and the ground state in ^{120}Sn have been extensively studied. The $E2$ (quadrupole) transition probabilities in ^{120}Sn are found to be fairly consistent with one another [12–17] with smaller uncertainties. However, the $E3$ probabilities have a wide range with larger uncertainties [12,18–20]. For the rotationally deformed ^{7}Li, transition to the only bound excited state of the nucleus prior to its breakup threshold has been well investigated [21–30], with the results for the $E2$ transition probability reasonably consistent in each measurement. The analysis of elastic and inelastic cross sections for $^7\mathrm{Li} + {}^{120}\mathrm{Sn}$ system at energies around the Coulomb barrier have been reported previously [31], similar to the present investigation, though not as extensive, where the main objective was to only measure the inelastic scattering angular distribution of the 2_1^+ state of ^{120}Sn for several ^{7}Li beam energies and study the effects of coupling transfer partitions to elastic and inelastic channels. References [32,33] also report similar inelastic scattering measurements for this reaction but at an energy much above the Coulomb barrier and a very limited angular coverage. The present paper emphasizes on the measurement of not only the rotational excitation of ^{7}Li but also the two vibrational states, 2^+ and 3^-, of ^{120}Sn to probe the $B(E2)$ and $B(E3)$ strengths.

Another dominant peripheral reaction channel is the transfer process. A single-nucleon transfer reaction can populate certain category of states in a very selective manner that have a structure predominantly given by the parent nucleus as a bound core, with the transferred nucleon in an orbit around it, populating any of its vacant higher levels to give rise to corresponding states of the residual nucleus, by coupling to the core ground state. Significant mixing may also occur between different simple configurations that all have the same spin and parity and about the same (unmixed) energy. As a result, such a single-particle state produced by a nucleon orbiting the core of the target, in an otherwise vacant orbital, will be mixed with other nuclear states of different structures. The state of the composite contains components of many single-particle states coupled to all possible core states, with each having a definite coefficient of fractional parentage (spectroscopic amplitude) [10,34]. The strength or probability of the population of each state depends on the intensity of this single-particle component, essentially known as the spectroscopic factor, $S_{\ell sj}^{J_i J_f}$, i.e., the probability of finding the nucleon in a single-particle state ℓ, s, j (spin J_f) coupled to the core with spin J_i. Experimentally, it is extracted by comparing the measured differential cross sections and those calculated for a pure single particle state. For such a transfer process involving a single nucleon, the initial target and final recoil states have definite isospin associated with them. Consequently, the spectroscopic amplitude is multiplied by an isospin Clebsch-Gordon coefficient, C [10,35]. The experimental and calculated cross sections are related as

$$\left(\frac{d\sigma}{d\Omega}\right)_{\mathrm{expt}} = \frac{2J_f+1}{2J_i+1} C^2 S_t C^2 S_p \left(\frac{d\sigma}{d\Omega}\right)_{\mathrm{calc}}, \tag{2}$$

where, in the case of the present system, C^2S_p and C^2S_t correspond, respectively, to the projectile-stripping and target-pickup overlaps $\langle {}^7\mathrm{Li}|{}^6\mathrm{Li}+n\rangle$ and $\langle {}^{120}\mathrm{Sn}+n|{}^{121}\mathrm{Sn}\rangle$ for the (^{7}Li,^{6}Li) reaction, and $\langle {}^7\mathrm{Li}|{}^6\mathrm{He}+p\rangle$ and $\langle {}^{120}\mathrm{Sn}+p|{}^{121}\mathrm{Sb}\rangle$ for the (^{7}Li,^{6}He) reaction. Studies of heavy-ion induced single-nucleon transfer reactions also reveal strong J and Q preferential selectivity in the relative cross sections, which primarily depends on the type of projectile and the orbit from which the transfer occurs [36–38]. In the present study as well, among the large number of known levels in the residual nuclei, up to ∼17 MeV excitation energy each in ^{121}Sn and ^{121}Sb, only some groups of levels are found to be enhanced that are favored by the selectivity conditions. Earlier measurements also exist on the population of states in ^{121}Sn and ^{121}Sb by means of light-ion bombardment, for instance ^{120}Sn[(t,d),(d,p)] [39–41] and ^{120}Sn[(^{3}He,d),(α,t)][42–44] reactions, respectively. In contrast to such light ion nucleon transfer reactions where the proton-neutron orbit has an s state for its initial bound orbital, the initial nucleon orbit is $p_{3/2}$ each for the (^{7}Li,^{6}He) and (^{7}Li,^{6}Li) reactions. As a result, the present reactions populate states in recoil nuclei with different strengths, based on the kinematic selection rules. Following the prescription given in Ref. [36], higher spin states are favored for the more negative Q values of the present reactions, as compared to the earlier measurements. Certain groups of states are enhanced over others, and the information about structural parameters of all such dominant states is essential to ascertain the validity and energy independence of their simultaneous description.

All current approaches to the extraction of realistic coupling parameters, like deformation parameters from inelastic excitations and spectroscopic information from heavy-ion transfer reactions, are based on the DWBA analysis of the CRC framework, the success of which is well established for energies above Coulomb barrier, to exploit the features of these reactions.

The paper is organized as follows. In Sec. II, the details of the experimental setup used to obtain the differential cross sections is described. The methods of analysis used to arrive at the experimental results are highlighted in Sec. III. The CRC calculations, via FRESCO, that represent the experimental data, along with relevant structural parameters, are described in Sec. IV, and finally, the results are discussed and summarized in Sec. V.

II. EXPERIMENTAL DETAILS

The angular distributions for elastic, inelastic, and transfer cross sections were measured at the BARC-TIFR Pelletron

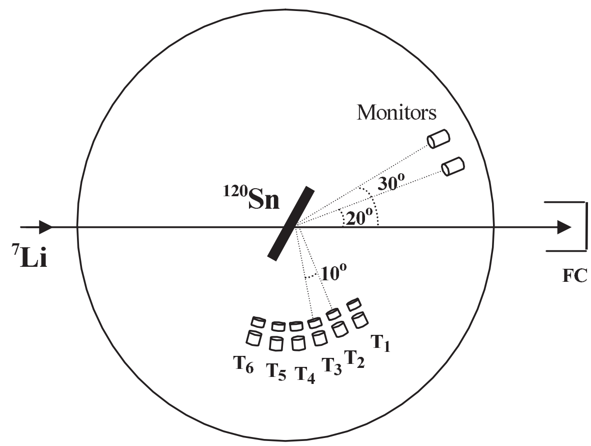

FIG. 1. Schematic of experimental setup

accelerator facility, Mumbai. A self-supporting enriched (∼99%) target of ^{120}Sn (thickness ∼280 μg/cm^2) was used. Six telescopes ($\Delta E - E$) of Si-surface barrier detectors, T_1–T_6, each placed 10° apart at a distance of ∼21 cm from the center of the scattering chamber, were used to detect the projectile-like fragments in the angular range of 25° to 140°. Two single Si-surface barrier detectors (monitors), fixed at 20° and 30° with regard to the beam at a distance of ∼39 cm from the center of the scattering chamber, were used for flux normalization. The detector thicknesses were typically 25 to 50 μm for ΔE and ∼1000 μm for the E detectors. A schematic of the setup is shown in Fig. 1.

From a typical gain-matched two-dimensional spectrum of ΔE vs $E + \Delta E$ shown in Fig. 2, the projectile-like fragments with different $Z(= 1$–$3)$ and $A(= 1$–$8)$ are clearly identified. Typical energy resolution of a telescope was ∼60 keV. The one-dimensional projection spectra corresponding to ^{7}Li, ^{6}Li, and ^{6}He particle bands with respect to their reaction Q values are shown in Figs. 3(a), 3(b), and 3(c) respectively. In Fig. 3(a), the elastic peak along with several inelastic states of projectile and target are observed. The inelastic states corresponding to

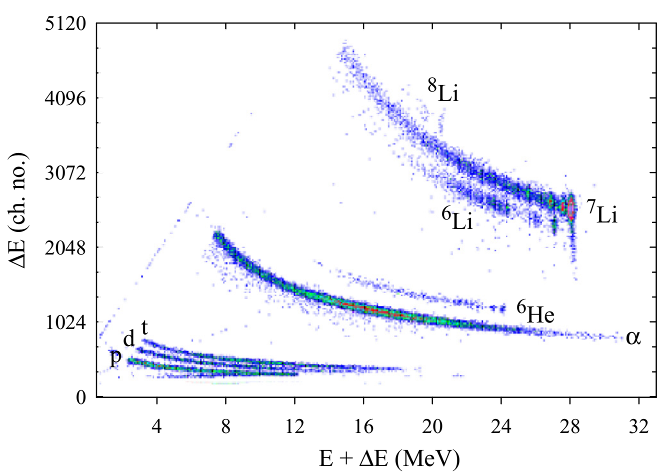

FIG. 2. Typical two-dimensional gain-matched spectrum showing the outgoing projectile-like fragments at $\theta_{\text{lab}} = 60°$.

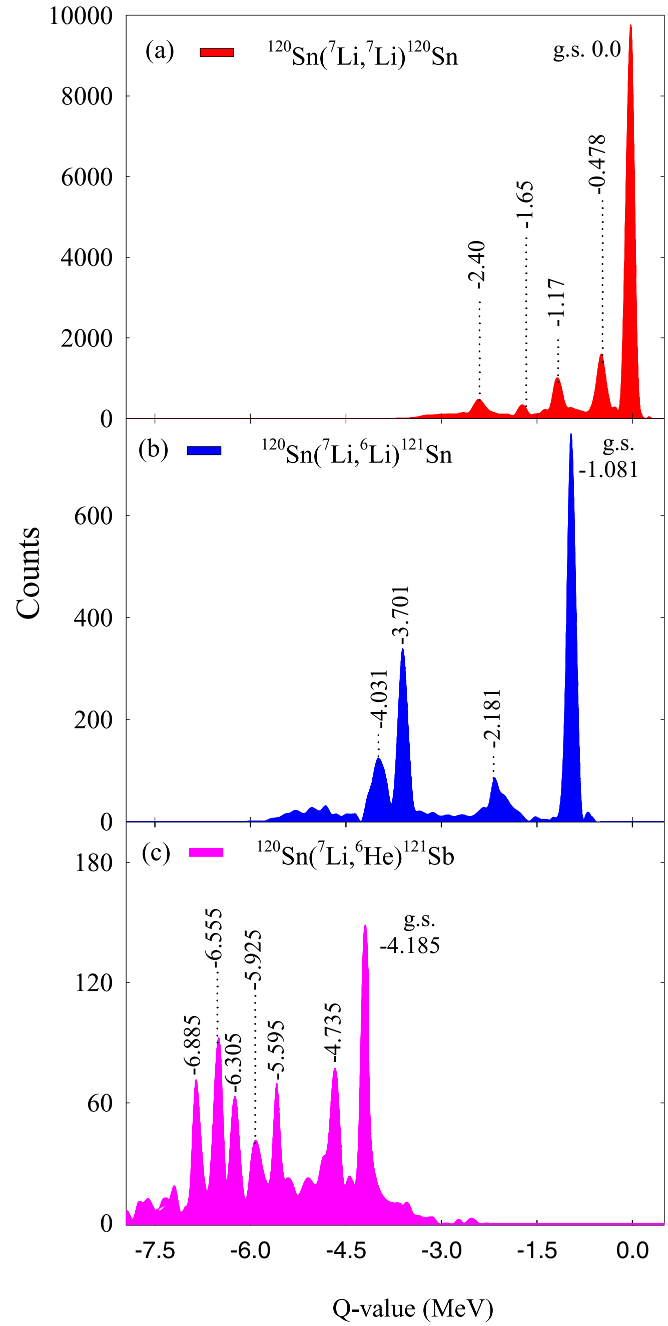

FIG. 3. Typical 1D spectrum showing Q-value distribution of states identified in (a) elastic and inelastic scattering, (b) 1n stripping transfer, and (c) 1p stripping transfer processes at $\theta_{\text{lab}} = 60°$.

first quadrupolar rotational state of ^{7}Li (0.478 MeV) and 2_1^+ quadrupole and 3_1^- octupole vibrational states of ^{120}Sn (at 1.17 and 2.40 MeV respectively) were found to be dominant. The mutual excitation of the first excited states of ^{7}Li and ^{120}Sn, at a Q value of −1.65 MeV, was also detected, though with low statistics. Figure 3(b) corresponds to the projection of ^{6}Li produced in 1-neutron stripping reaction, i.e., (^{7}Li,^{6}Li), with ground-state Q value of −1.0809 MeV. In addition to the ground state, three more 1n transfer states corresponding to the excitations (1.10, 2.63, and 2.95 MeV) of the residual

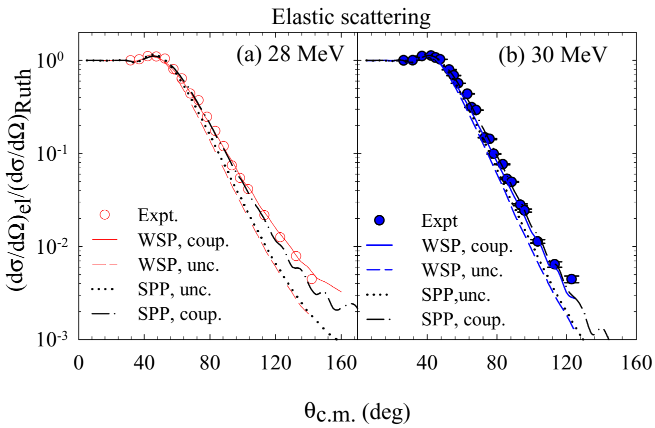

FIG. 4. Experimental cross section and CRC calculation for the elastic channel (relative to Rutherford).

nucleus ^{121}Sn with their respective Q values of −2.181, −3.701, and −4.031 MeV are identified and their yields are extracted for obtaining the cross sections. Similarly, Fig. 3(c) corresponds to the projection of ^{6}He band produced in 1-proton stripping reaction, i.e., (^{7}Li,^{6}He), with a ground-state Q value of −4.185 MeV, and several excitations of the residual nucleus ^{121}Sb with Q values in the range of −4.735 to −6.885 MeV could be identified.

III. DATA ANALYSIS AND RESULTS

In the analysis, the yields for the elastic, inelastic, and all the identified states of the transfer partitions were extracted separately for evaluating their respective experimental differential cross sections. While the inelastic peaks could be clearly identified corresponding to particular excitations of projectile and target, for the case of the densely populated transfer peaks, each centroid could contain contributions from more than one state that may be embedded within a background of other nuclear levels, owing to the existence of several closely spaced neighboring states in both the residual nuclei. Few groups of states are found to be enhanced over others.

All the angular distributions were first obtained in the laboratory frame, and then translated to the center-of-mass frame using the prescription described in Ref. [45]. The experimental differential cross sections in the center-of-mass system for elastic, inelastic, $1n$ stripping, and $1p$ stripping reactions have been shown as open (filled) circles for $E_{\rm beam} = 28$ (30) MeV in Figs. 4, 5, 6, and 7 respectively. The statistical errors on the elastic scattering cross sections are typically 1–2% over the entire angular range, except at extreme backward angles, where it ranges between 4 and 5% for both energies. The error bars remain within the size of the data points, except for a few points at backward angles. The inelastic cross sections corresponding to the excitations of (i) ^{7}Li ($1/2^-$, 0.478 MeV), (ii) ^{120}Sn (2^+, 1.17 MeV), (iii) ^{7}Li ($1/2^-$, 0.478 MeV) + ^{120}Sn (2^+, 1.17 MeV) together, and (iv) ^{120}Sn (3^-, 2.40 MeV) are respectively plotted in Figs. 5(a)–5(d) for 28 MeV and in Figs. 5(e)–5(h) for 30 MeV. The lines in Figs. 4 and 5 represent the results of coupled-channels calculations described in Sec. IV.

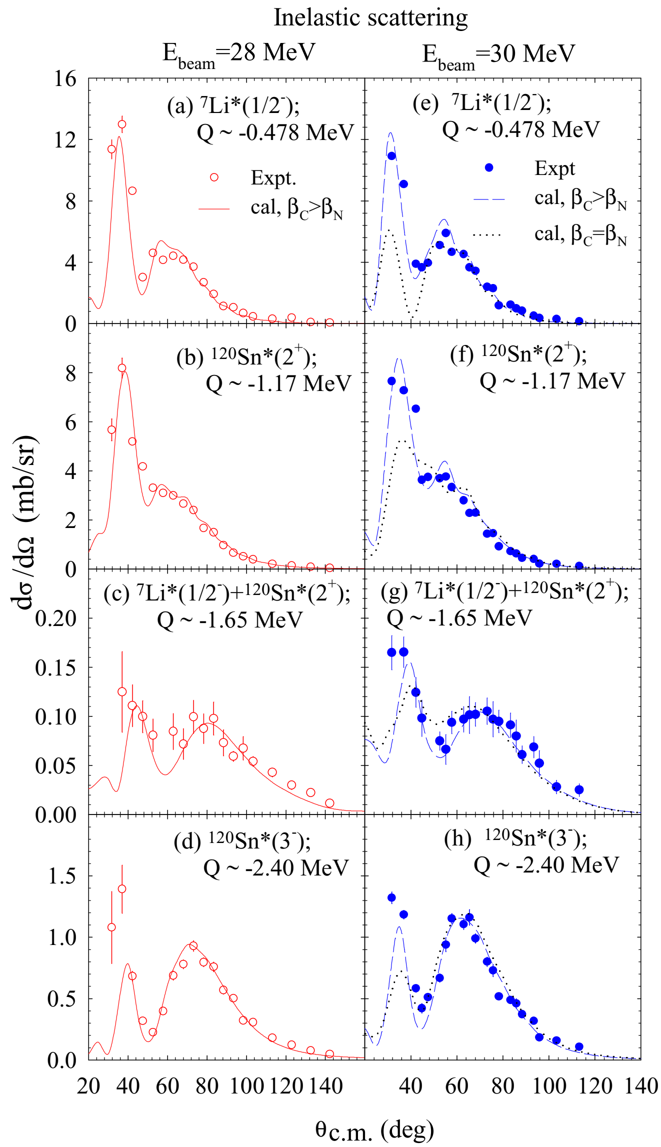

FIG. 5. Experimental cross sections (open circles) and respective calculations (solid lines) for inelastic scattering processes in ^{7}Li + ^{120}Sn system at 28 MeV for (a) quadrupole excitation in ^{7}Li, (b) quadrupole excitation in ^{120}Sn, (c) mutual quadrupolar transitions in ^{7}Li and ^{120}Sn, and (d) octupole excitation in ^{120}Sn. The corresponding experimental data (filled circles) and calculations (dashed lines) for 30 MeV are shown in panels (e), (f), (g), and (h), respectively. Dotted lines in panels (e)–(h) represent calculations for $E_{\rm beam} = 30$ MeV using modified but equal Coulomb and nuclear deformation lengths.

For $1n$ stripping, i.e., ^{120}Sn(^{7}Li,^{6}Li)^{121}Sn reaction, the differential cross sections have been obtained from the yields under four different peaks with different excitation energies of the residual nuclei. For all the four cases, ^{6}Li is in its ground state but ^{121}Sn is in ground as well as excited states. The first peak from the right in Fig. 3(b) with a Q value of −1.081 MeV corresponds to the ground states of both ^{6}Li and ^{121}Sn along with 6- and 60-keV excitations of ^{121}Sn. The second peak with observed excitation energy of 1.10 MeV (Q value = −2.181 MeV) corresponds to the combination of

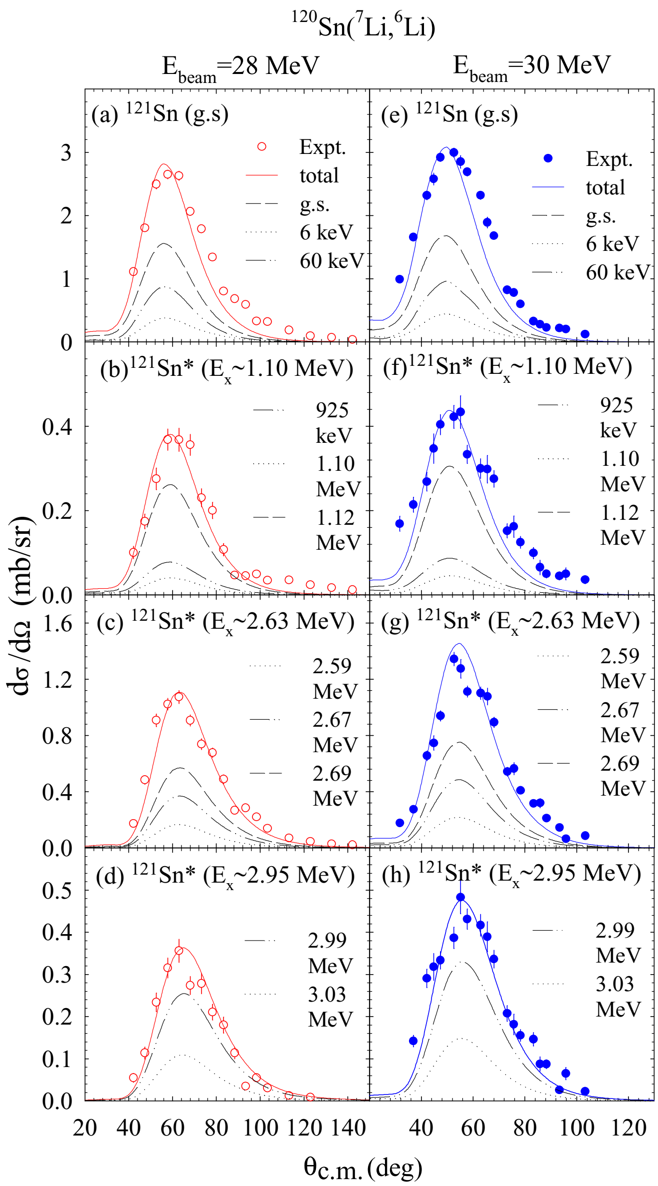

FIG. 6. Experimental cross sections (open circles) and respective CRC calculations (lines) for $1n$ transfer process (^{7}Li,^{6}Li) at 28 MeV for different excitations of the recoiling nucleus are shown in panels (a)–(d). Solid lines represent total contributions from experimentally unresolved multiple states with individual cross sections shown by dotted, dash-dot-dotted, and dashed lines. The corresponding experimental data (filled circles) and calculations (lines) for 30 MeV are shown in panels (e)–(h). The structural information of the states included in the model calculations for each centroid energy are listed in Table III.

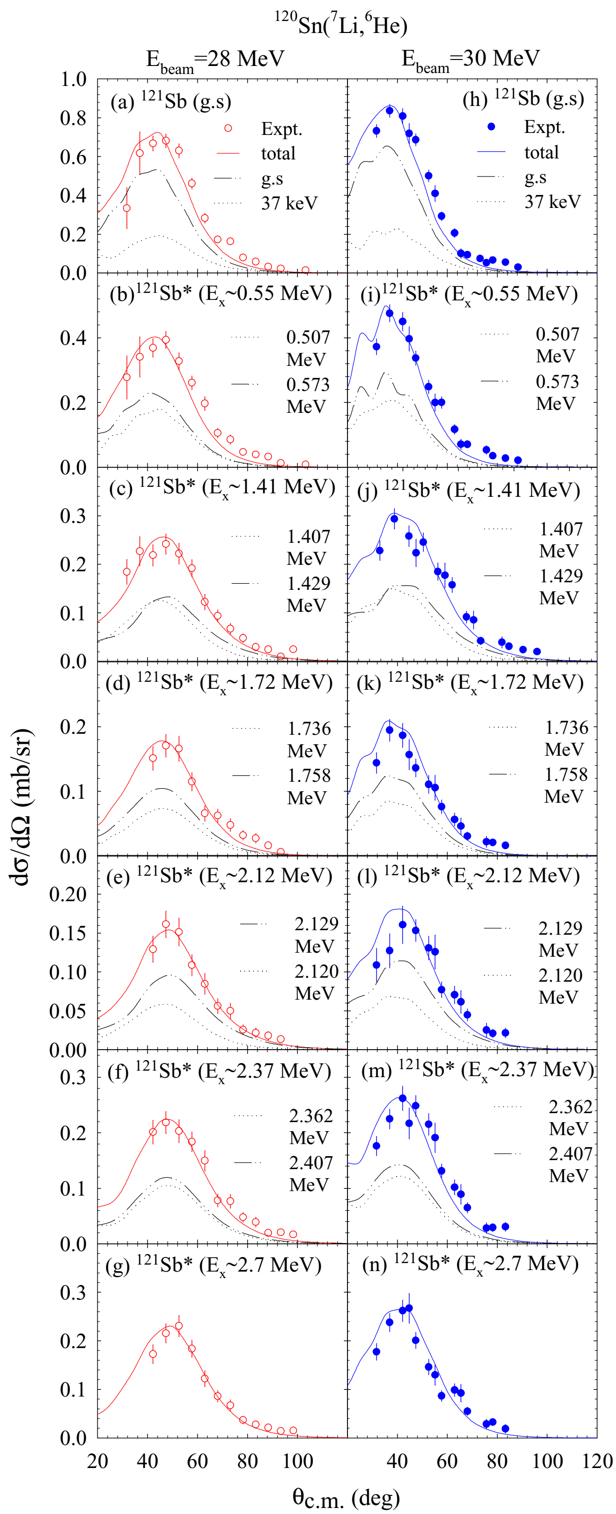

FIG. 7. Experimental cross sections (open circles) and CRC calculations (lines) for $1p$ transfer process (^{7}Li,^{6}He) at 28 MeV for different excitations of the recoiling nucleus are shown in panels (a)–(g). Solid lines represent total contributions from experimentally unresolved multiple states with individual cross sections shown by dotted and dash-dot-dotted lines. The corresponding data (filled circles) and calculations (lines) for 30 MeV are shown in panels (h)–(n). The structural information of the states included in the model calculations for each centroid energy are listed in Table III.

three close-by excited states of ^{121}Sn with ($7/2^+$, 0.925 MeV), ($3/2^+$, 1.101 MeV), and ($5/2^+$, 1.121 MeV). The third peak with observed excitation energy of 2.63 MeV (Q value $= -3.701$ MeV) corresponds to the combination of three close-by excited states of ^{121}Sn with ($7/2^-$, 2.589 MeV), ($3/2^-$, 2.666 MeV), and ($7/2^-$, 2.690 MeV). Similarly, the fourth peak with observed excitation energy of 2.95 MeV (Q

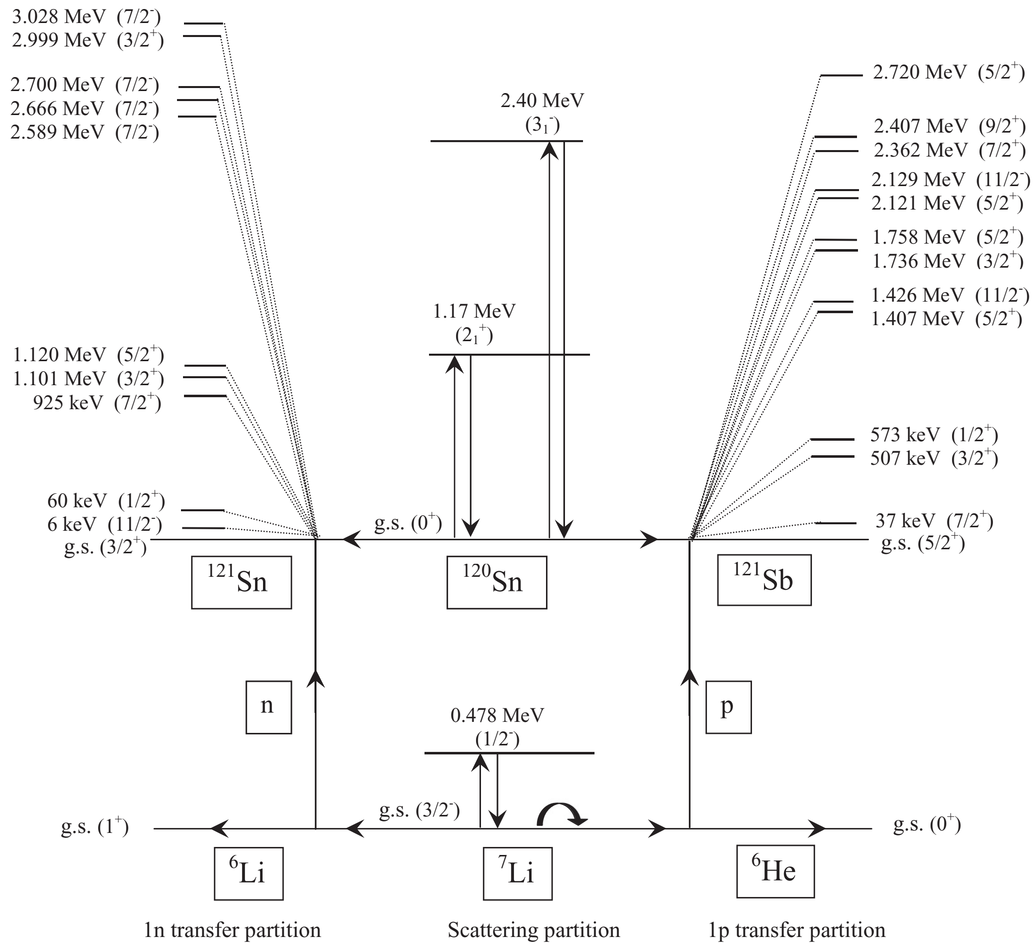

FIG. 8. Coupling scheme used for the CRC calculations by FRESCO.

value = −4.031 MeV) corresponds to the combination of two close-by excited states of ^{121}Sn with ($3/2^+$, 2.999 MeV) and ($7/2^-$, 3.028 MeV). The respective experimental differential cross sections are shown as open circles in Figs. 6(a)–6(d) for 28 MeV and filled circles in Figs. 5(e)–5(h) for 30 MeV.

Similarly, for $1p$ stripping, i.e., ^{120}Sn(^{7}Li,^{6}He)^{121}Sb reaction, the differential cross sections have been obtained from the yields under seven different peaks with observed excitation energies of 0.0, 0.55, 1.41, 1.74, 2.12, 2.37, and 2.70 MeV. These excitations correspond to the states of ^{121}Sb with (i) ($5/2^+$, g.s.) + ($7/2^+$, 0.037 MeV), (ii) ($3/2^+$, 0.507 MeV) + ($1/2^+$, 0.573 MeV), (iii) ($5/2^+$, 1.407 MeV) + ($11/2^-$, 1.426 MeV), (iv) ($3/2^+$, 1.736 MeV) + ($5/2^+$, 1.758 MeV), (v) ($5/2^+$, 2.120 MeV) + ($11/2^-$, 2.129 MeV), (vi) ($7/2^+$, 2.362 MeV) + ($9/2^+$, 2.407 MeV), and (vii) ($5/2^+$, 2.72 MeV) with ^{6}He in its ground state for all the cases. The respective experimental differential cross sections are shown as open circles in Figs. 6(a)–6(g) for 28 MeV and as filled circles in Figs. 5(h)–5(n) for 30 MeV.

The lines plotted in Figs. 6 and 7 represent the results of coupled-channels calculations described in the following section.

IV. CRC CALCULATIONS

CRC calculations in DWBA limit were performed by including the major direct reaction channels (as many as 30 significant channels) that couple to the entrance channel (see Fig. 8), and the results are compared with the experimental data for both energies. Simultaneous description of elastic, inelastic, and one-nucleon transfer has been attempted by using the same set of potential as well as structural parameters. The attempt here was to utilize the structure information (deformation parameters for inelastic states and spectroscopic factors for the transfer partitions) already available in the literature and predict the cross sections for all identified states, consistently at both energies. However, for a few of the channels, these structural parameters were either unavailable or had to be varied to obtain optimum representation of experimental data.

The coupling of all possible open reaction channels to the entrance channel is essentially manifested into the elastic scattering cross section. From the phenomenological optical model analysis of elastic scattering data (normalized to Rutherford), the nuclear potential employed was of Woods-Saxon form, whose depth was adjusted to simultaneously fit the elastic, inelastic, and transfer cross sections for all observed states at

TABLE I. WS potential parameters for entrance channel used in OM fit and CRC calculation.

Model calculation	V_0 (MeV)	r_0 (fm)	a_0 (fm)	W_0 (MeV)	r_w (fm)	a_w (fm)
OM fit	24.7	1.243	0.695	57.7	1.138	0.678
CRC	35.1	1.243	0.695	57.7	1.138	0.678

both energies. The total potential is defined as

$$U(r) = V_c(r,r_c) - \frac{V_0}{1+\exp\left(\frac{r-r_0}{a_0}\right)} - \frac{W_0}{1+\exp\left(\frac{r-r_w}{a_w}\right)}. \tag{3}$$

Here, $V_c(r,r_c)$ is the Coulomb potential due to a uniformly charged sphere of radius $R_c = r_c(A_P^{1/3} + A_T^{1/3})$, with r_c fixed at 1.2 fm and A_P and A_T are the mass numbers of projectile and target, respectively. The optical model (OM) fit to the elastic scattering data (not shown in the figure) at both energies was first carried out by varying all six parameters of the nuclear potential of Woods-Saxon volume form. The potential parameters used for OM fit of only elastic scattering data without any coupling are listed in Table I. However, by including the coupling of nonelastic channels to elastic channel, the final CRC calculations that provides the best description of elastic as well as nonelastic channels required a modified depth of the real potential as given in the Table I. The enhanced strength of the real potential in CRC calculation was required to take care of the effect of coupling of the inelastic and transfer channels.

As ^{7}Li is a weakly bound projectile, the coupling to its continuum (i.e., breakup channels) along with bound inelastic states of projectile and target and transfer channels is ideal. However, due to the limitation of coupled-channels code FRESCO, the simultaneous coupling of both target inelastic states as well as projectile continuum channels is prohibitive [31]. So, the present calculations include only the bound inelastic and transfer channels and no breakup channel is considered. Similarly there could be some transfer channels which are left out due to computational limitation. Since every single nonelastic channel could not be incorporated into the calculations, a volume absorptive imaginary potential with the parameters given in Table I was used to account for flux lost from elastic channel into those nonelastic direct channels that had been excluded from the calculations, like breakup, multinucleon transfer, etc. This volume imaginary potential also accounts for the compound reaction in the entrance channel.

In addition to the elastic channel, the same phenomenological real potential has been used for the identified direct reaction channels in CRC calculations to explain the experimental differential cross sections and subsequently extract the relevant structural parameters from each. The inelastic states were treated as collective vibrational and rotational states, for the target and projectile, respectively. A short-ranged imaginary potential of Woods-Saxon square form, given by $V_0 = 10.00$ MeV, $r_0 = 1.00$ fm, and $a_0 = 0.40$ fm, has also been used in the exit channels of the transfer partitions to account for the absorption of flux from these channels at short range. The potentials binding the transferred particles were of Woods-Saxon volume form, with radius $1.25A^{1/3}$ fm and diffuseness 0.650 fm, with A being the mass of the core nucleus. The depths were automatically adjusted to obtain the required binding energies (separation energies) of the particle-core composite system. Integrating the radial wave functions up to 40 fm in steps of 0.25 fm and summing over 100 partial waves were found to be adequate to attain convergence of the calculations for the current angular range of interest.

The results of FRESCO calculations for elastic scattering angular distributions using the above potentials, shown as solid lines in Figs. 4(a) and 4(b) for 28 and 30 MeV, respectively, reproduce the experimental data well. The dashed lines represent the results without any coupling. In order to compare the calculations using above phenomenological potentials with some universal potential, the CRC calculations have also been carried out using Sao Paulo potential (SPP) [46] with both real and imaginary parts. It was observed that the uncoupled calculations using SPP are able to reproduce the experimental elastic scattering reasonably (not shown in the figure). However, the full CRC calculations including dominant inelastic and transfer channels require the real part of the SPP to be increased by a factor of 1.4 in order to explain the measured elastic scattering. The results of the elastic scattering cross sections using SPP with increased real potential have been shown in Fig. 4 as dash-dotted and dotted lines corresponding to calculations with and without coupling respectively.

The results of CRC calculations for elastic, inelastic, and transfer angular distributions discussed in the following sections and shown in Figs. 5, 6, 7, and 9 have been obtained using the phenomenological potentials described above.

A. Inelastic cross sections

For the inelastic scattering, the upward reduced electric transition probabilities quoted in the literature with various probes could not effectively reproduce the experimental data throughout the angular range, thereby indicating a qualitative probe dependence (static and dynamic effects) of the collective nature of such transitions, particularly beyond the Coulomb-nuclear interference region. This was particularly significant for the octupole collectivity in ^{120}Sn. For the quadrupolar transition in ^{120}Sn, the electric transition probability extracted from the Coulomb deformation parameter (β_C) in the forward region is consistent with already available measurements; also, the previously measured values of ground-state quadrupole moment (reorientation coupling) as well as upward transition probability to the bound excited state for ^{7}Li could reasonably reproduce the corresponding forward angle data extracted from the present measurement. These parameters could also effectively reproduce the mutual excitation of the first excited states in both projectile and target in this region, thereby emphasizing their validity. However, by keeping the charge and matter deformation lengths same, the nuclear contribution to the scattering could not be reproduced (in the region beyond the minima position); i.e., the electric transition probabilities used so far are unable to explain the data over the complete angular range. As a consequence, while the

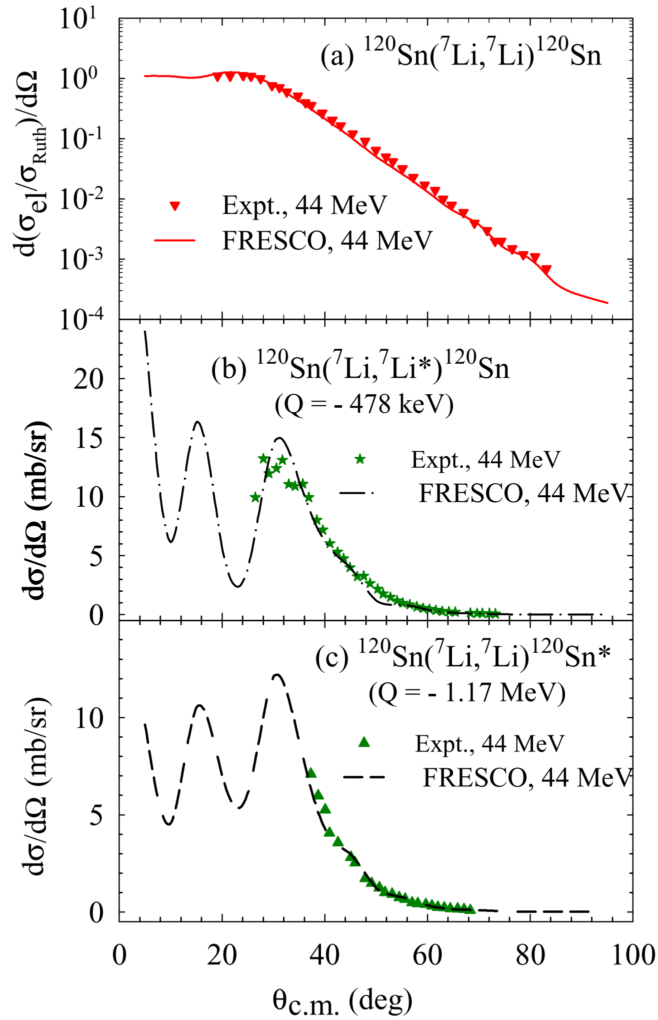

FIG. 9. Available data at $E_{\text{beam}} = 44$ MeV, for (a) elastic scattering and (b) inelastic scattering corresponding to the 478-keV excitation of ^{7}Li from Ref. [32] and (c) inelastic scattering corresponding to the 1.17-MeV state in ^{120}Sn taken from Ref. [33]. The lines represent the model calculations.

$B(E\lambda)$ values that primarily depend on the proton transition matrix element [8,47] could be suitably used to generate optimum representation of experimental data in the forward region, they may fail to reproduce the cross sections over the entire angular range, and a different multipole parameter may be required [48,49] to account for the effect of the nuclear field and its interference with the Coulomb field. The nuclear deformation parameters (β_N) obtained by normalizing to the data for each excitation were found to be lower than their respective Coulomb counterparts, thereby leading to a difference between the charge and matter distributions for the same nucleus under consideration. For the case of the octupole transition in ^{120}Sn, the highest value of $B(E3;\ ^{120}\text{Sn}\ (0_1^+ \to 3_1^-)) = 0.159$ e^{2}b^3 quoted in literature [19] could not explain the population of this excited state even in the forward region, while normalizing to the data in the nuclear region gave a value of the nuclear (matter) deformation parameter as 0.0957(56). This indicates the existence of significant projectile-target

TABLE II. Deformation parameters from inelastic excitations.

Nucl.	E_x (MeV)	λ	β_C	β_N (fm)	$\beta_C R_C$ (fm)	$\beta_N R_N$ (fm)
^{7}Li	0.48	2	1.718(61)	0.885(52)	3.944 (141)	1.993 (107)
^{120}Sn	1.17	2	0.112(6)	0.107(7)	0.662 (29)	0.624 (35)
^{120}Sn	2.40	3	0.161	0.0957(56)	0.953	0.556 (29)

structure-dependent effects, particularly into the excitation of the octupole state in the target. These transition probabilities offer a test for nuclear structure effects involved in these scatterings, as they involve the wave functions of the initial and final states. The parameters were optimized to represent both the energies and the optimum values deduced from the present work give reasonable representation of the data: $B(E2;\ ^7\text{Li}(3/2^- \to 1/2^-)) = 8.39(26)$ e^2 fm^4, with ground-state intrinsic quadrupole moment for ^{7}Li as 20.56(81) e fm^2, and $B(E2;\ ^{120}\text{Sn}(0_1^+ \to 2_1^+)) = 0.213(8)$ e^2 b^2. These extracted values are consistent to within 5–6% with literature-quoted values. The nuclear and Coulomb deformation parameters for each nucleus are compared in Table II.

The experimental data along with calculations for all these states are shown in Fig. 5. The solid (dashed) lines in Fig. 5 represent the results of FRESCO calculations for inelastic cross sections at $E_{\text{beam}} = 28$ (30) MeV using unequal nuclear and Coulomb deformation lengths. With optimized deformation parameters, the peaks of inelastic scattering shifts to lower scattering angle, with higher magnitude, for the higher of the two energies. Typical calculations for $E_{\text{beam}} = 30$ MeV using modified but equal Coulomb and nuclear deformation lengths ($\beta_N R_N = \beta_C R_C$) are also shown by dotted lines in Fig. 5 to show the difficulty in explaining both forward and backward angle maxima of the experimental data simultaneously.

B. One-nucleon transfer cross sections

On the other hand, the transfer angular distributions are peaked in the vicinity of the grazing angle for the collision at each energy. For ^{120}Sn(^{7}Li,^{6}Li)^{121}Sn and ^{120}Sn(^{7}Li,^{6}He)^{121}Sb reactions, the transferred neutron and proton, respectively, come from the $p_{3/2}$ orbit of ^{7}Li. The structures of the residuals are essentially dominated by these single-particle degrees of freedom coupled to vibrations of the spherical Sn core, i.e., by coupling the odd proton or odd neutron in the spherical shell model orbitals $2d_{5/2}$, $1g_{7/2}$, $3s_{1/2}$, $2d_{3/2}$, and $1h_{11/2}$ to the low-lying excitations of the Sn cores [50].

The amplitude for the overlaps $\langle ^7\text{Li}|^6\text{Li} + n\rangle$ and $\langle ^7\text{Li}|^6\text{He} + p\rangle$ are taken as 0.948 [51] and 0.768 [52], respectively. Comparisons between calculations and experimental data fix the quantum numbers of the final states of the residual nuclei as well as the spectroscopic factors denoting the overlap between initial and final states. In the limit of detector resolution, due to mixing of indistinguishable closely spaced neighboring states in both recoils, the angular distribution for each peak was represented by a group of kinematically allowed states in the calculations around that particular reaction Q value. For some of the states included in the calculations, whose total angular momenta are unknown, they were assigned

TABLE III. Particle-core spectroscopic factors for the $1n$ and $1p$ transfer states in residual nuclei.

Nucleus	E_x (expt.) (MeV)	E_x (calc.) (MeV)	State ($n\ell j$)	$C^2S_{\ell j}$	Ref.	$C^2S_{\ell j}$ (present work)
^{121}Sn	g.s.	0.00	$2d_{3/2}$	0.439	[40]	
		0.006	$1h_{11/2}$	0.488	[40]	
		0.060	$3s_{1/2}$	0.315	[39]	
	1.10	0.925	$1g_{7/2}$	0.049	[39]	
		1.101	$2d_{3/2}$	0.0125	[39]	
		1.121	$2d_{5/2}$	0.066	[39,41]	
	2.62	2.589	$2f_{7/2}$	0.052	[39]	
		2.666	$2f_{7/2}$	0.119	[39]	
		2.690	$2f_{7/2}$	0.185	[41]	
	2.95	2.999	$2d_{3/2}$			0.151(12)
		3.028	$2f_{7/2}$	0.041	[40]	
^{121}Sb	g.s.	0.00	$2d_{5/2}$	0.915	[43]	
		0.037	$1g_{7/2}$	1.13	[44]	1.277(91)
	0.55	0.507	$2d_{3/2}$	0.295	[43]	0.375(17)
		0.573	$3s_{1/2}$	0.379	[43]	0.484(33)
	1.41	1.407	$2d_{5/2}$	0.183	[42,43]	
		1.426	$1h_{11/2}$	1.12	[44]	1.021(69)
	1.74	1.736	$2d_{3/2}$			0.143(10)
		1.758	$2d_{5/2}$			0.152(12)
	2.12	2.120	$2d_{5/2}$	0.085	[43]	
		2.129	$1h_{11/2}$			0.648(51)
	2.37	2.362	$1g_{7/2}$			0.504(42)
		2.407	$1g_{9/2}$			0.522(48)
	2.70	2.72	$2d_{5/2}$	0.185	[43]	0.348(31)

the highest spin possible for the known angular momentum transfer, in accordance with kinematic selection rules for this system. While most of the spectroscopic factors are taken from literature [39–41,43,44], some have been adjusted to reproduce the data, with the majority agreeing to within 20–30% with the existing values, and few have been extracted exclusively in the present work. Extracted spectroscopic factors are obtained primarily by normalization in the region of the grazing angle. For the angular distribution represented by more than one excited state of the residual nucleus, the state with the higher cross section is assigned a higher value of modified or new spectroscopic factor. The channels included in the calculations are listed in Table III, with respective structural information.

The angular distributions of experimental data along with CRC calculations are shown for $1n$ transfer in Fig. 6 and for $1p$ transfer in Fig. 7. The solid lines represent the sum of the theoretical cross sections corresponding to one or more closely spaced states which were experimentally unresolved. The individual cross sections of the constituent states have also been shown in the above figures by dotted, dash-dotted, and dashed lines. Details of the constituent states corresponding to each of the experimental peaks are given in Table III.

C. Calculations for existing data at 44 MeV

In order to further verify the extracted set of potential and coupling parameters, an attempt was made to reproduce existing data, if any, on elastic, inelastic, and transfer cross sections for the ^{7}Li + ^{120}Sn system at different energies. There are only a few measurements available in the literature [31,32,53] for this system. Sousa *et al.* [53] have measured the angular distributions for the quasielastic scattering in the present system. The data includes, in addition to elastic channel, the contributions from inelastic scattering corresponding to the excitations of ^{7}Li*($1/2^-$, 0.478 MeV) and ^{120}Sn*(2^+, 1.17 MeV) and the transfer reaction ^{120}Sn(^{7}Li,^{6}Li)^{121}Sn$_{g.s.}$. So, comparison of this data with CRC calculations is unexpected to yield any meaningful information. In the paper by Zagatto *et al.* [31], the available data are elastic scattering and one inelastic scattering corresponding to the 2_1^+ excited state of ^{120}Sn at around barrier energies. Although the elastic scattering data could be well reproduced using the same set of potential coupling parameters and the coupling scheme as used in the above coupled-channels calculations, the inelastic scattering cross sections were overpredicted compared to the experimental data. It may be noted that the inelastic scattering angular distributions in Ref. [31] were obtained from the coincidence yields of de-excitation γ rays and scattered projectile-like fragments, a method different from the present work.

In another work, Tungate *et al.* [32] have measured the angular distributions, at 44 MeV beam energy, for elastic scattering and inelastic scattering corresponding to ^{7}Li*($1/2^-$, 0.478 MeV) excitation. While the inelastic data for excitation to the 2_1^+ state of ^{120}Sn($E_x = 1.17$ MeV) are available in Ref. [33], at the same beam energy, though with limited angular coverage. These measurements at 44 MeV for the elastic and two highly dominant direct channels of this system could be effectively reproduced with the same set of potential and structural parameters and coupling the same number of reaction channels as done for 30 and 28 MeV. The results are depicted in Figs. 9(a)–9(c) as solid, dash-dotted, and dashed lines respectively for elastic scattering and inelastic scattering corresponding to ^{7}Li*($1/2^-$, 0.478 MeV) and ^{120}Sn*(2^+, 1.17 MeV) excitations. This puts emphasis on the validity of the realistic coupling parameters extracted in the present study.

V. DISCUSSION AND SUMMARY

Differential cross sections for elastic, four inelastic, and eleven nucleon-transfer channels in the ^{7}Li + ^{120}Sn system have been measured at two beam energies at 28 and 30 MeV. A simultaneous description of the experimental cross sections with realistic structural parameters has been attempted through a single coupled-channel formalism by coupling around 30 exit channels to the entrance channel within the DWBA limit. For the inelastic scattering, the Coulomb deformation parameter, associated with $B(E\lambda)$, characterizes the shape of the deformed charge distribution of the nucleus when transitions of multipolarity λ take place. On the other hand, the nuclear deformation parameter contains the mass (protons + neutrons) contributions to the excitation. It will be equal to its Coulomb counterpart if protons and neutrons contribute in the ratio Z/N [8,54]. For the excitations in both projectile and target, differences are observed between the Coulomb and nuclear deformations. The neutron and proton collective contributions are different, indicating different transition densities. While pure Coulomb excitation probes proton matrix elements, heavy-ion scattering like in the present study is sensitive to both proton and neutron degrees of freedom and gives realistic deformation parameters over the entire angular range (range of impact parameters). The $B(E2)$ values for $\lambda = 2$ excitations in ^{7}Li and ^{120}Sn were found to be consistent with existing measurements. However, the wide range of $B(E3)$ values available in literature for ^{120}Sn could not reproduce experimental data at both energies.

The nuclear deformation parameter for all transitions was found to be significantly smaller than the charge deformation parameter for both projectile and target excitations. The net effects of all these couplings are manifested in the optical potential, the size and shape of which are the result of a convolution of projectile and target properties, and the reduced value of nuclear deformation may reflect the finite size of the projectile smearing out the deformation of the target nucleus and vice versa [11]. When sufficient overlap is present between masses of projectile and target, wave functions get damped quick enough owing to strong absorption, so that matter contributions to the scattering processes reduce [54].

For the transfer processes, the centroids of each of the identified states are represented by groups of states that may be mixed owing to the large density of neighboring states in the recoil nuclei. From the Q-value distribution, it is revealed that both the $1n$ and $1p$ transfer processes proceed mainly from the projectile and target ground states, and contributions from complex configurations involving target and/or projectile excited states are absent. The overlap amplitudes for the projectile-ejectile core-composite systems were taken from literature. While most of the target-residual spectroscopic factors could reproduce the experimental data at both energies, some had to be modified, with the majority agreeing to within ~30% of existing information, and some were assigned in this work for the first time. Realistic structural information is required for all inelastic and transfer channels for the system under consideration in order to test the validity of the model calculations.

To summarize, simultaneous description of elastic and several inelastic and transfer channels has been made for $^{7}\mathrm{Li} + {}^{120}\mathrm{Sn}$ system at 28 and 30 MeV and realistic structural information has been extracted for each channel, with a unique set of potential and coupling parameters at both energies. The spectroscopic factors for few states populated by 1-nucleon transfer have been exclusively assigned in the present work.

ACKNOWLEDGMENTS

We thank the Pelletron crew for smooth operation of the accelerator during the run. The financial support of BRNS through Project No. 2012/21/11-BRNS/1090 is gratefully acknowledged.

[1] F. Videbaeko, I. Chernov, P. Christensen, and E. E. Gross, Phys. Rev. Lett. **28**, 1072 (1972).

[2] J. P. Fernandez-Garcia, M. Cubero, L. Acosta, M. Alcorta, M. A. G. Alvarez, M. J. G. Borge, L. Buchmann, C. A. Diget, H. A. Falou, B. Fulton *et al.*, Phys. Rev. C **92**, 044608 (2015).

[3] M. Cubero, J. P. Fernandez-Garcia, M. Rodriguez-Gallardo, L. Acosta, M. Alcorta, M. A. G. Alvarez, M. J. G. Borge, L. Buchmann, C. A. Diget, H. A. Falou *et al.*, Phys. Rev. Lett. **109**, 262701 (2012).

[4] A. Sanetullaev, R. Kanungo, J. Tanaka, M. Alcorta, C. Andreoiu, P. Bender, A. A. Chen, G. Christian, B. Davids, J. Fallis *et al.*, Phys. Lett. B **755**, 481 (2016).

[5] E. Kwan, C. Y. Wu, N. C. Summers, G. Hackman, T. E. Drake, C. Andreoiu, R. Ashley, G. C. Ball, P. C. Bender, A. J. Boston *et al.*, Phys. Lett. B **732**, 210 (2014).

[6] H. T. Fortune and R. Sherr, Phys. Rev. C **85**, 051303 (2012).

[7] W. T. Pinkston and G. R. Satchler, Nucl. Phys. **27**, 270 (1961).

[8] A. M. Bernstein, V. R. Brown, and V. A. Madsen, Phys. Rev. Lett. **42**, 425 (1979).

[9] A. M. Bernstein, V. R. Brown, and V. A. Madsen, Phys. Lett. B **71**, 48 (1977).

[10] I. J. Thompson and F. M. Nunes, *Nuclear Reactions for Astrophysics* (Cambridge University Press, New York, 2009).

[11] W. Feix, W. Wilcke, T. Elze, H. Rebel, J. Huizenga, R. Thompson, and R. Dreizler, Phys. Lett. B **69**, 407 (1977).

[12] T. H. Curtis, R. A. Eisenstein, D. W. Madsen, and C. K. Bockelman, Phys. Rev. **184**, 1162 (1969).

[13] B. Hrastnik, V. Knapp, and M. Vlatkovic, Nucl. Phys. **89**, 412 (1966).

[14] P. Stelson and F. McGowan, Phys. Rev. **110**, 489 (1958).

[15] P. Stelson, F. McGowan, R. Robinson, and W. Milner, Phys. Rev. C **2**, 2015 (1970).

[16] R. Graetzer, S. Cohick, and J. Saladin, Phys. Rev. C **12**, 1462 (1975).

[17] J. Bryssinck, L. Govor, V. Y. Ponomarev, F. Bauwens, O. Beck, D. Belic, P. von Brentano, D. D. Frenne, T. Eckert, C. Fransen *et al.*, Phys. Rev. C **61**, 024309 (2000).

[18] N. G. Jonsson, A. Backlin, J. Kantele, R. Julin, M. Lountama, and A. Passoja, Nucl. Phys. A **371**, 333 (1981).

[19] O. Beer, A. E. Behay, P. Lopato, Y. Terrien, G. Vallois, and K. K. Seth, Nucl. Phys. A **147**, 326 (1970).

[20] G. Bruge, J. Faivre, H. Faraggi, and A. Bussiere, Nucl. Phys. A **146**, 597 (1970).

[21] G. J. C. V. Niftrik, L. Lapikas, H. D. Vries, and G. Box, Nucl. Phys. A **174**, 173 (1971).

[22] T. Davidson, V. Rapp, A. Shotter, D. Branford, M. Nagarajan, I. Thompson, and N. Sanderson, Phys. Lett. B **139**, 150 (1984).

[23] V. Hnizdo, K. W. Kemper, and J. Szymakowski, Phys. Rev. Lett. **46**, 590 (1981).

[24] W. J. Vermeer, A. M. Baxter, S. M. Burnett, M. T. Esat, M. P. Fewell, and R. H. Spear, Aust. J. Phys. **37**, 273 (1984).

[25] W. Vermeer, M. Esat, M. Fewell, R. Spear, A. Baxter, and S. Burnett, Phys. Lett. B **138**, 365 (1984).

[26] A. Weller, P. Egelhof, R. Caplar, O. Karban, D. Kramer, K. H. Mobius, Z. Moroz, K. Rusek, E. Steffens, G. Tungate *et al.*, Phys. Rev. Lett. **55**, 480 (1985).
[27] F. C. Barker, Y. Kondo, and R. Spear, Aust. J. Phys. **42**, 597 (1989).
[28] P. Egelhof, W. Dreves, K. H. Mobius, E. Steffens, G. Tungate, P. Zupranski, D. Fick, R. Bottger, and F. Roesel, Phys. Rev. Lett. **44**, 1380 (1980).
[29] W. Vermeer, R. Spear, and F. Barker, Nucl. Phys. A **500**, 212 (1989).
[30] H. G. Voelk and D. Fick, Nucl. Phys. A **530**, 475 (1991).
[31] V. A. B. Zagatto, J. R. B. Oliveira, L. R. Gasques, J. A. Alcantara-Nunez, J. G. Duarte, V. P. Aguiar, N. H. Medina, W. A. Seale, K. C. C. Pires, A. Freitas *et al.*, J. Phys. G: Nucl. Part. Phys. **43**, 055103 (2016).
[32] G. Tungate, D. Kramer, R. Butsch, O. Karban, K. H. Mobius, W. Ott, P. Paul, A. Weller, E. Steffens, and K. Becker, J. Phys. G: Nucl. Phys. **12**, 1001 (1986).
[33] K. Becker, K. Blatt, H. J. Jansch, W. Korsch, H. Leucker, W. Luck, H. Reich, H. G. Volk, D. Fick, and K. Rusek, Nucl. Phys. A **535**, 189 (1991).
[34] C. Scheidenberger and M. Pfutzner (eds.), *The Euroschool on Exotic Beams* (Springer, Berlin, 2014), Vol. 4.
[35] S. K. Das, A. S. B. Tariq, A. F. M. M. Rahman, P. K. Roy, M. N. Huda, A. S. Mondal, A. K. Basak, H. M. Sen Gupta, and F. B. Malik, Phys. Rev. C **60**, 044617 (1999).
[36] F. Pougheon and P. Roussel, Phys. Rev. Lett. **30**, 1223 (1973).
[37] D. M. Brink, Phys. Lett. B **40**, 37 (1972).
[38] G. Morrison, J. Phys. Colloques **33**, C5-111 (1972).
[39] R. F. Casten, E. R. Flynn, O. Hansen, and T. J. Mulligan, Nucl. Phys. A **180**, 49 (1972).
[40] M. J. Bechara and O. Dietzsch, Phys. Rev. C **12**, 90 (1975).
[41] E. J. Schneid, A. Prakash, and B. L. Cohen, Phys. Rev. **156**, 1316 (1967).
[42] M. Conjeaud, S. Harar, and Y. Cassagnou, Nucl. Phys. A **117**, 449 (1968).
[43] T. Ishimatsu, K. Yagi, H. Ohmura, Y. Nakajima, T. Nakagawa, and H. Orihara, Nucl. Phys. A **104**, 481 (1967).
[44] J. P. Schiffer, S. J. Freeman, J. A. Caggiano, C. Deibel, A. Heinz, C. L. Jiang, R. Lewis, A. Parikh, P. D. Parker, K. E. Rehm *et al.*, Phys. Rev. Lett. **92**, 162501 (2004).
[45] L. I. Schiff, *Quantum Mechanics*, 1st ed. (McGraw-Hill, New York, 1949), Vol. 2.
[46] L. C. Chamon, Nucl. Phys. A **787**, 198 (2007).
[47] A. M. Bernstein, V. R. Brown, and V. A. Madsen, Phys. Lett. B **103**, 255 (1981).
[48] G. M. Ukita, T. Borello-Lewin, L. B. Horodynski-Matsushigue, J. L. M. Duarte, and L. C. Gomes, Phys. Rev. C **64**, 014316 (2001).
[49] S. T. Thornton, T. C. Schweizer, D. E. Gustafson, J. L. C. Ford, Jr., and M. J. Levine, Nucl. Phys. A **270**, 428 (1976).
[50] D. Bucurescu, I. Cata-Danil, G. Ilas, M. Ivascu, L. Stroe, and C. A. Ur, Phys. Rev. C **52**, 616 (1995).
[51] J. P. Schiezer, G. C. Morrison, R. H. Siemssen, and B. Zeidman, Phys. Rev. **164**, 1274 (1967).
[52] S. Cohen and D. Kurath, Nucl. Phys. A **101**, 1 (1967).
[53] D. Sousa, D. Pereira, J. Lubian, L. Chamon, J. Oliveira, E. R. Jr., C. Silva, P. de Faria, V. Guimaraes, R. Lichtenthaler *et al.*, Nucl. Phys. A **836**, 1 (2010).
[54] M. Baranger and E. Vogt (eds.), *Advances in Nuclear Physics* (Springer, New York, 1969), Vol. 3.